Residual stress distribution in a Ti-6Al-4V T-joint weld measured using synchrotron X-ray diffraction

Xu, L.[a], Zhang, S.Y.[b], Sun, W.[c*], McCartney, D.G.[c], Hyde, T.H.[c], James, J.[d], and Drakopoulos, M.[e]

a. TWI Ltd.,Granta Park, Great Abington, Cambridge CB21 6AL, U.K.
b. ISIS Facilities, Science and Technology Facilities Council, Oxford OX1 10QX, U.K.
c. Division of Materials, Mechanics and Structures, University of Nottingham, Nottingham NG7 2RD, U.K.
d. Department of Materials Engineering, Open University, Milton Keynes MK7 6AA, U.K.
e. Diamond Light Source Ltd, Harwell Science and Innovation Campus, Oxford, OX11 0DE, U.K.

*Corresponding author: w.sun@nottingham.ac.uk, Division of Materials, Mechanics and Structures, University of Nottingham, Nottingham NG7 2RD, U.K.

Abstract

To improve the manufacturing quality of welded structures, to prevent failures at weld joints and to predict their lifetime, measurements of the residual stresses generated by welding in the structures are extremely useful. ~~The residual stresses may reduce the component life due to phenomena that occur at low applied stresses such as brittle fracture, fatigue and stress corrosion cracking.~~ Welded thin Ti-6Al-4V panel components are commonly found in aero-engine assemblies and the weld integrity and reliability are critical. In this work, the residual stress distributions in a welded thin Ti-6Al-4V T-joint were measured by the newly developed SScanSS program with synchrotron X-ray diffraction technique. The measurement performed in this study, which included a large number of measurement points, has mapped a complete stress field in a thin sheet T-joint weld. It has not only provided improved understanding of residual stress in such a joint but also filled the missing link between the residual stress obtained by numerical modelling and their validation. The results have shown that the longitudinal stresses play the most important role in the residual stress distribution over the flange and high tensile stresses appear in the region near the weld zone. The measured results were compared with numerically predicted results and these showed good agreement.

Keywords: Ti-6Al-4V T-joint, residual stress, diffraction, synchrotron X-ray, finite element

1. Introduction

Welding-induced residual stress is one of the most important issues in fusion welding fabrication [1]. Due to heating, melting and cooling during welding, plastic thermal strain occurs close to the weld region which results in permanent deformation. Thermally induced stresses are caused by the high rates of heating and cooling which produce fast changing temperature gradients in the materials. If the workpiece is not properly restrained, the thermally induced stresses could cause significant distortions of the workpiece. However, if the workpiece is completely or partially restricted in order to reduce the distortions, the

unbalanced thermally induced stresses could lead to more significant residual stresses. The residual stress in welded structures may cause phenomena that can reduce component life under low applied stresses such as brittle fracture, fatigue and stress corrosion cracking [1]. Therefore, these stresses can result in significant increase in manufacturing and repair costs and also limit the development of innovative designs.

To minimise the welding-induced residual stresses, welding preparation, welding sequence, fixture design, heat treatment and other practical methods are used. Numerical simulation techniques have also been developed to predict the residual stresses generated by welding and thus to identify the optimum welding sequence/procedure to minimise the residual stress [1-7]. With the aid of the practical approach and the computational tool, the controlled and minimised residual stress can help to reduce manufacturing cost, improve component life and enable novel component design. However, fundamental understanding of the welding-induced residual stress distribution in typical welded structures, which provides baseline data to the practical technique and computational method, must be established.

In this work, residual stresses in a Ti-6Al-4V T-joint produced by robotic keyhole plasma arc welding (K-PAW) were measured by synchrotron X-ray diffraction. The titanium alloy T-joint was designed as a representative joint feature of welding fabrication in an aero-engine. The K-PAW process is extensively employed as one of the primary joining methods of metal components in aerospace high value manufacturing [8]. Synchrotron X-ray diffraction has in recent years become a more widely used non-destructive method to determine residual stresses within the bulk of materials [9]. The measurements took place at the Diamond Light Source, Rutherford Appleton Laboratory, United Kingdom, using the beamline I12-JEEP.

Although recent advances in synchrotron X-ray diffraction permit a far more detailed and accurate measurement of weld residual stress fields, previous diffraction measurement research [10-15] were performed in heavy gauge materials (12 to 30 mm thick) with only a small number of measurement positions (20 to 50 points). In addition, the materials which had been looked at were not in the category of aerospace alloys. Despite that, their target materials were not the general aerospace alloys, particularly in the synchrotron X-ray diffraction measurements. A previous study [16] reported a residual stress measurement study of a thin (3 mm thick) stainless steel bead-on-plate sample by neutron diffraction. However, the nature of the weld sample made it difficult to represent a real joint in actual welding production, which caused limitations in the use of measurements to resolve real-world welding matters. The measured sample in this work represented the material and joint features of a demonstrator for production aerospace component and was welded using representative production equipment. The measurement results have mapped the complete stress field in the welded sample using a large number of measurement points. This is the first experiment performed at I12 using the SScanSS [19] virtual laboratory to help with the experimental setup.

The experimental procedure for the residual stress measurement is firstly presented in this paper. Then the results of the measurement are discussed along with the comparison with published results of finite element modelling.

2. Experimental work

2.1 Overview of synchrotron X-ray diffraction

By delivering high flux and high brightness of the synchrotron X-ray, the instrument provides researchers with a powerful method for ~~the purpose of~~ non-destructive experimental characterisation. The beamline I12-JEEP (Figure 1), powered by a 4.2 T superconducting multi-pole wiggler, generates a wide, smooth spectrum of X-rays with useable X-ray photon energy range from 50 to 150 keV [17]. The instrument is an automated programmable measurement system.
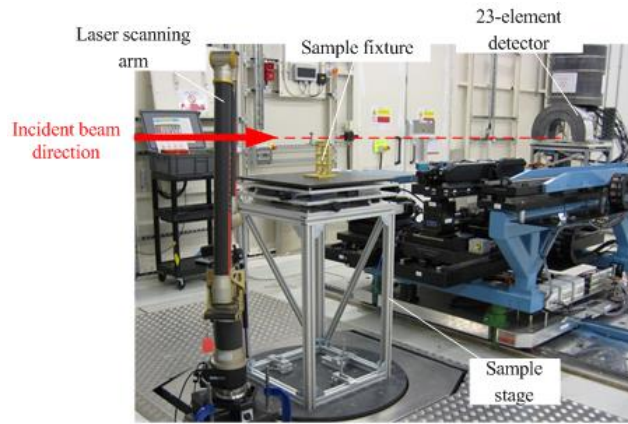
Figure 1 Experiment hutch of beamline JEEP at Diamond Light Source.

~~The s~~ Synchrotron X-ray diffraction measures the lattice spacing of a crystalline material. The crystal lattice spacing in the strain free material is used as an internal strain gauge and thus the lattice strain on a group of parallel lattice planes (*hkl*) can be determined. If there is any stress acting on the crystal lattice, the corresponding lattice spacing will be different from that of its unstrained condition. Therefore, the strain on a group of lattice planes, ε_{hkl}, can be calculated as shown in Equation 1:

$$\epsilon_{hkl} = \frac{d_{hkl} - d_{hkl}^0}{d_{hkl}^0} \qquad (1)$$

where *hkl* denotes the parallel lattice planes, d_{hkl} the lattice spacing between neighbouring parallel lattice planes in the strained condition, d_{hkl}^0 the lattice spacing between neighbouring parallel lattice planes in the unstrained condition.

Then the strains and stresses can be related to the stress by the Hooke's Law:

$$\sigma_{ij} = \frac{E}{1+v} \left(\varepsilon_{ij} + \frac{v}{1-2v} \, \delta_{ij} \, \varepsilon_{kk} \right) \qquad (2)$$

where E is the Young's modulus, v the Poisson's ratio, ε_{ij} the strain tensor, σ_{ij} the stress tensor, δ_{ij} the Kronecker delta (i.e. $\delta_{ij} = 1$ when $i = j$, and $\delta_{ij} = 0$ when $i \neq j$), and ε_{kk} the sum over all *kk*.

2.2 Material and sample

Welded Ti-6Al-4V sheets in the format of T-joint were investigated in this study, as shown in Figure 2 (flange: $150 \times 80 \times 2.1$ mm, and web: $150 \times 48 \times 2.1$ mm). The thickness of the sheets was 2.1 mm and the joint was formed by two partially overlapped passes. All the welds were produced at the University of Nottingham using a robotic welding cell. As seen in Equation 1, to obtain the residual strains in the material, the lattice spacing d_{hkl}^0 in the material's unstrained condition is required. The d_{hkl}^0 was obtained by measuring the unstrained (d^0) samples which were cut from another T-joint weld with identical material, dimensions, welding procedure, using electric discharge machining (EDM) wire cutting. The EDM wire cutting technique was used to conduct the cutting and it is assumed that this will not introduce additional stress inside the surrounding material. As the heating and cooling cycles along the welding directions are different, this can cause differences which will affect the lattice spacing. In order to improve the accuracy of measurement, two d^0 samples with a thickness of 5 mm were cut from the sample at the weld start and middle, respectively (Figure 2). By cutting the two 5 mm thick slices from the sample, the longitudinal (*Y-Y*) stresses were released. Then the two slices were cut into a 'comb' shape in the flange and a 'fish bone' shape in the web using the EDM cutting with an ultra-fine wire (diameter 0.1 mm), as shown in Figure 3. After the cut of the 'comb and fish bone' shapes, the transverse (*X-X* in flange, *Z-Z* in web) stresses in the d^0 samples is assumed to reduce to a negligible level. Therefore, the 'strain-free' status of the d^0 samples was believed to be approximately achieved, which enables the measurements taken on the d^0 samples to be used as the reference in the later stress calculation.
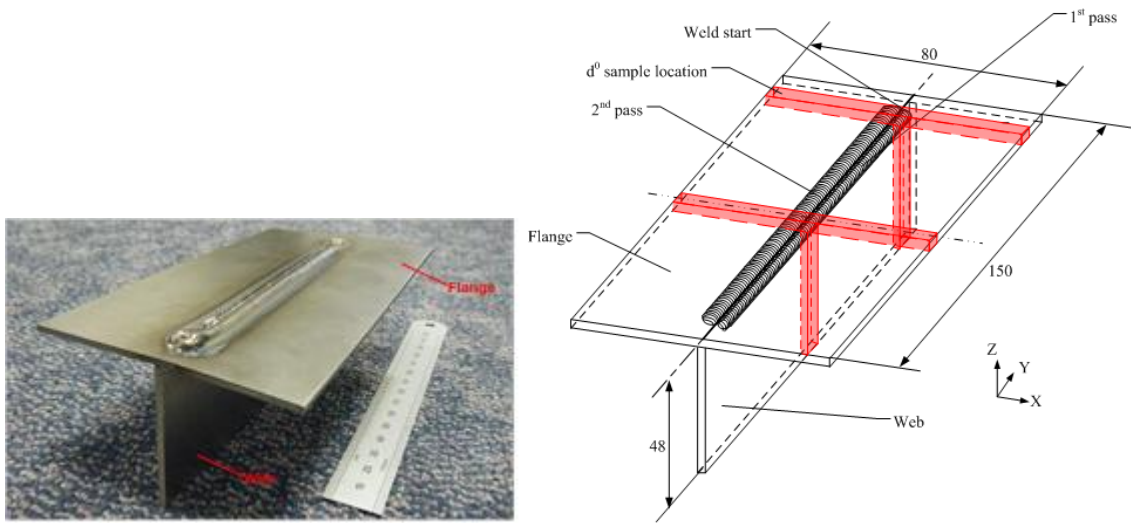

Figure 2 Schematic drawing of Ti-6Al-4V flat T-joint weld measured by synchrotron X-ray diffraction.
Red-coloured potions are the locations where the strain-free samples were cut.
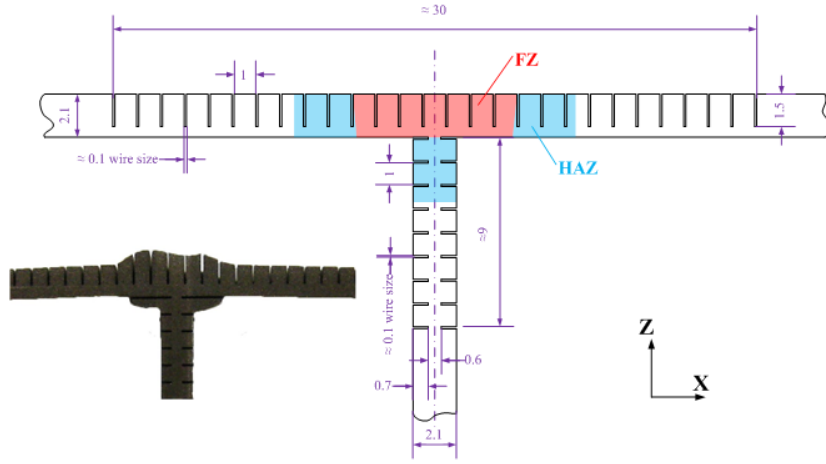The thickness of each strain-free (d^0) sample was 5 mm. Values are in mm.

Figure 3 Cross-section of 'comb and fish bone' strain-free (d^0) sample for synchrotron X-ray diffraction residual stress measurement in Ti-6Al-4V flat T-joint sample. Values are in mm.
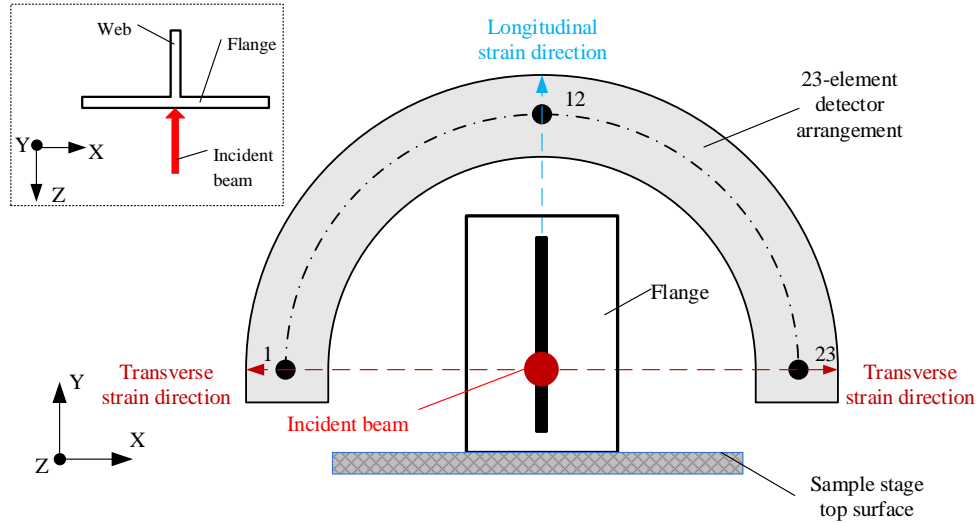
2.3 Experiment set-up

In the thin sheet weld, since the internal loading is mainly in-plane, there are only relatively small stresses acting normal (Figure 2, Z-Z direction in flange, X-X direction in web) to the sheet surfaces. Therefore, the strains normal to the sample surfaces were ignored in the measurement in order to save the limited beamtime. During the welding manufacture, the flange sheet was sitting on the top of the web, with the welding arc running on the top surface of the flange. Although the arc penetrated through the flange and melted a small part of the web top, compared with the flange, the heat transfer interaction between the arc and the web was still much less than that between the arc and the flange. Thus the residual stresses due to the non-uniform rapid heating and cooling in the web are expected to be much less intensive than in the flange. As a result, the focus of the measurements was placed on the flange in terms of the longitudinal (Y-Y) and the transverse (X-X) strains.

Synchrotron X-ray experiments were carried out at the Diamond light source, on I12 [22]. The beamline uses a 4.2 T superconducting wiggler to provide white beam and monochromatic X-rays in the energy range 50–150 keV. The experiment was performed in the white beam energy dispersive mode, which allowed multiple Bragg peaks to be measured simultaneously. Samples were scanned through a rectangular beam that had the vertical aperture of 0.05mm (along y axis in Figure 4a), horizontal aperture of 0.05mm (along x axis) and receiving slit before the detector of 0.1 mm. Giving the diffraction angle of 2θ=5°, length of the gauge volume is approximately 1.7mm in z direction (size of D in Figure 4b). 23-element energy dispersive detectors were arranged in a semi-annular array. The sample position and detectors used are shown in the Figure 4a. Detector element 1 and 23 were used to measure transverse strain and element 12 were used to measure longitudinal strain. The acquisition time for a single measurement point was 2 minutes. A typical diffraction pattern is shown in Figure 4b.

As indicated in Figure 4c, diffraction measurements were carried out to determine the longitudinal (Y-Y) and transverse (X-X) strain components along a set of parallel transverse (X-X) lines in the flange. As shown in Figure 4d, since the gauge volume size (approximately 1.7 mm long) is only slightly smaller than the plate thickness (2.1 mm), each measurement

point was placed at the middle of the thickness (1.05 mm below the flange top surface) to ensure that the gauge volume was completely inside the material, which was to optimise the measurement accuracy. Therefore, longitudinal and transverse stress maps covering the complete flange X-Y region could be obtained from the measurement. Furthermore, the d^0 samples were measured at the middle point on each 'comb' tooth in the flange across the parent material, heat-affected zone, and fusion zone up to the parent material at the other end. The careful measurement coverage of all zones in the d^0 samples was to ensure the chemical and structural composition changes due to the intensive heating and rapid cooling of welding were taken into consideration.
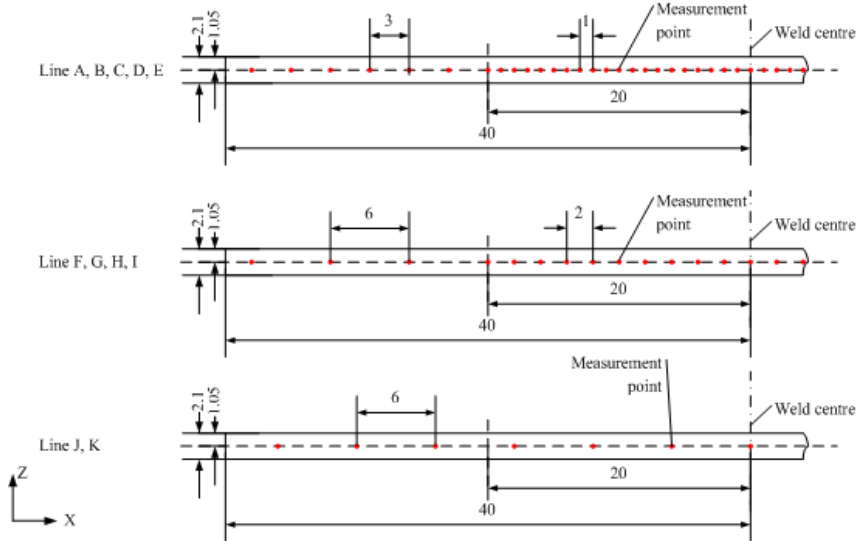

(a)
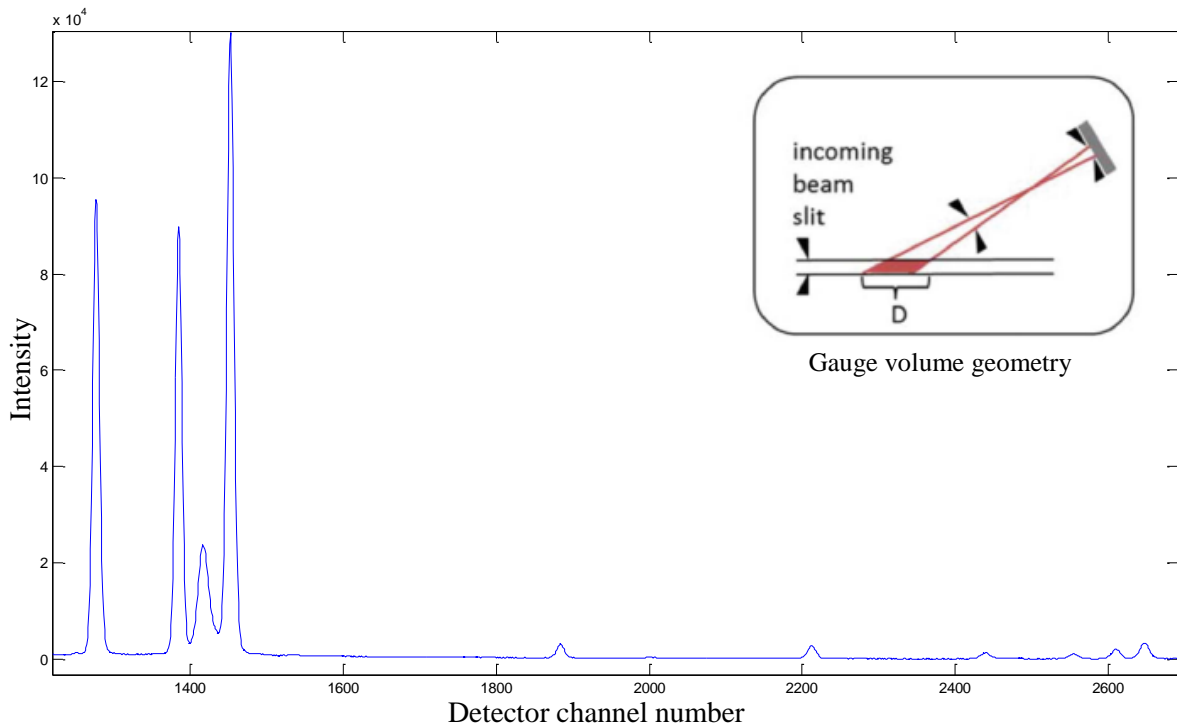
(b)
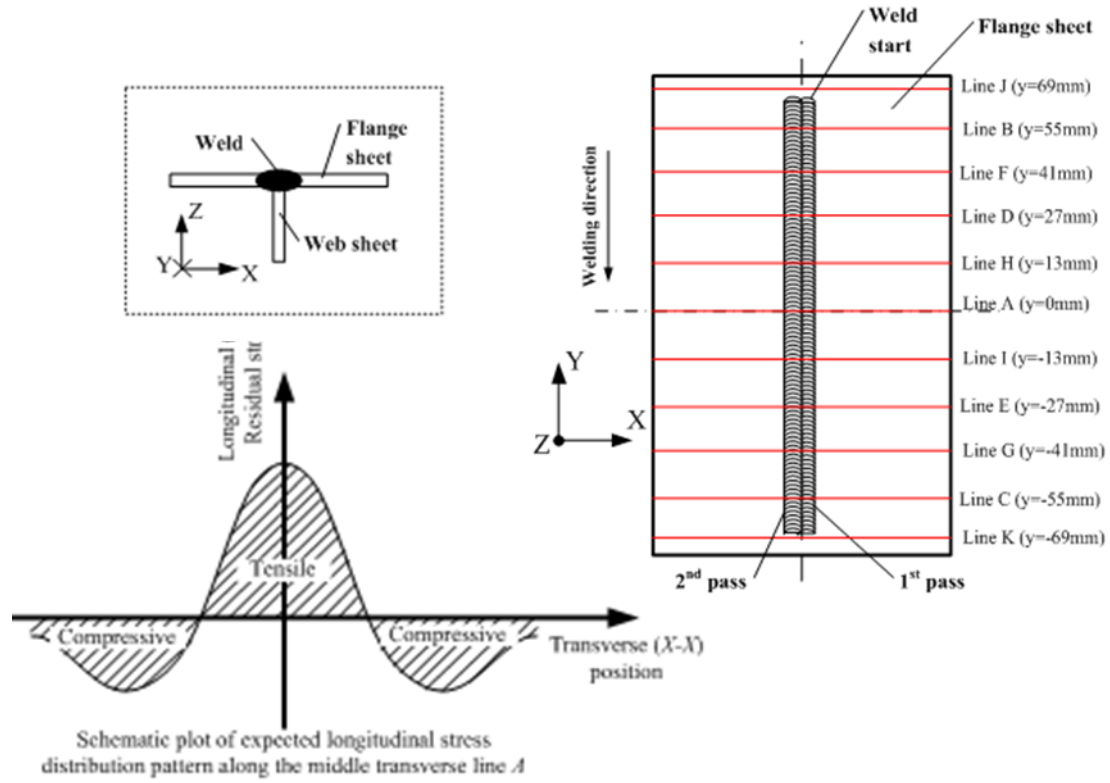
(c)

(d)

Figure 4 Measurement plan in Ti-6Al-4V flat T-joint weld: (a) experimental setup (b) diffraction pattern of Ti-6Al-4V; (c) measurement points located along parallel transverse lines indicated in red colour and schematic pattern of expected longitudinal stress distribution along Line A; (d) through-thickness view of measurement point locations (the arrangement of points is symmetrical about the weld centre line so only half of the through-thickness cross-section is displayed).

Due to the small thickness of the component and the non-uniformly distorted component profile, accurate positioning of the sample for each measurement was potentially difficult.

This difficulty was overcome by using the **S**train **Scan**ning **S**imulation **S**oftware SScanSS, [18,19]. This software is widely used for planning, optimising and controlling residual stress measurements on neutron diffraction instruments, but this is the first time the approach has been used on a synchrotron instrument. The software provides a virtual laboratory, allowing a sample model, in this case a laser scan of the component, to be combined with an accurate kinematic virtual instrument model. Measurement points and strain components are defined on the virtual sample in the sample coordinate system. The sample position on the real instrument is then determined by measuring the position, in the instrument coordinate system, of a number of fiducial markers attached to the sample. This information is input to the software thereby setting up the correspondence between the real and virtual laboratories. The accuracy of the correspondence is confirmed by requiring the system to bring particular features, such as the fiducial markers, to the instrument measurement point and checking that it has done so. The software was developed with the aim of maximising efficient use of beam-time by facilitating planning, minimising setup time and avoiding problems such accidental collisions between moving instrument components. Automatic calculation of path lengths can be used to minimise attenuation and reduce measurement times.

3. Results and Discussion

3.1 Residual stresses in the Ti-6Al-4V T-joint weld

For each synchrotron X-ray measurement point, the diffraction spectra containing all the peaks were obtained by the detectors. The measurement data were translated to lattice spacing values and then used to obtain strain data from the strain free measurement values. Given that the strain-free lattice spacing was determined as a function of position across the parent material, heat-affected zone and fusion zone, the residual elastic strain and stress distributions in the flange could be calculated. As the insignificant stresses normal to the plate surface were ignored in the measurement, the stress calculation did not consider the normal stresses. The macroscopic value of *Young's* modulus *E* used in the calculation was 113.8 GPa and the Poisson's ratio *v* was 0.342 based on the data from literature [20].

The longitudinal and transverse residual stress variations are plotted as a function of position in Figures 5 and 6, respectively. The labels of the measurement lines in the figures refer to the ones defined in Figure 4. To provide a better overview of the longitudinal and transverse residual stress fields over the measured layer 1.05 mm below the flange top surface, contours are plotted in Figures 7 and 8. As seen in the figures, the residual stress patterns in both the longitudinal and the transverse directions follow similar trends which indicate that larger stress magnitudes occur around the first weld pass rather than the second weld pass. This is because the first weld pass experiences two rapidly changing intensive thermal cycles when the welding arc passes through it but the second pass has only one.
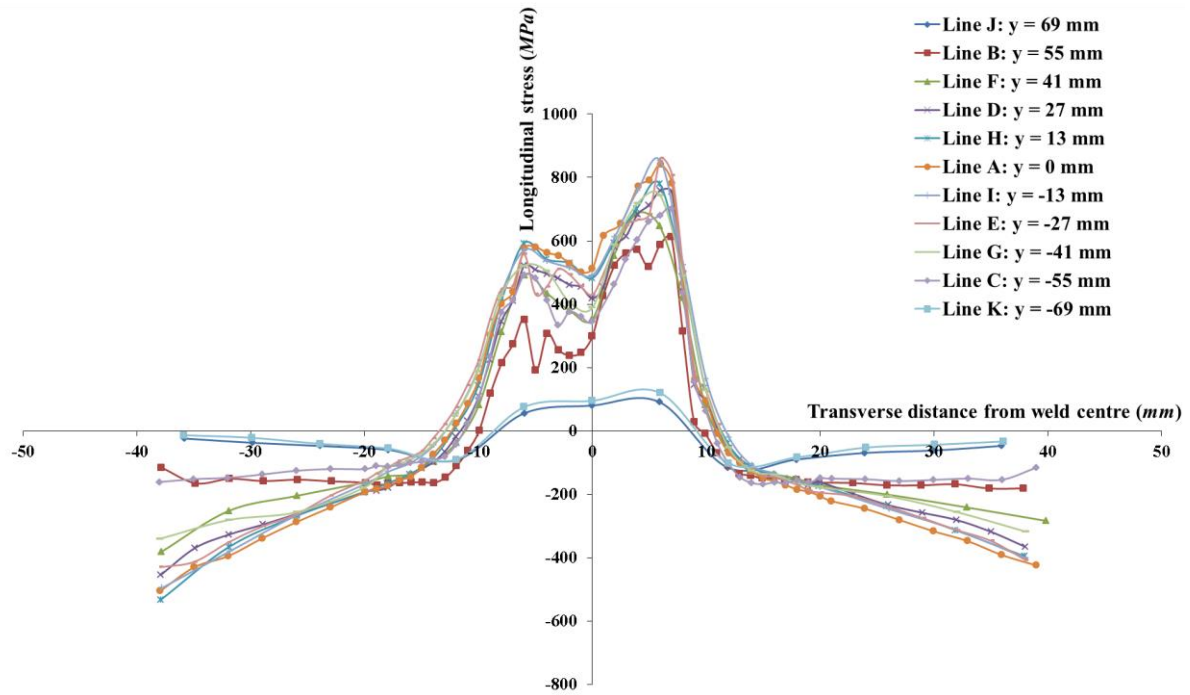
Figure 5 Longitudinal residual stresses along all measurement lines in Ti-6Al-4V flat T-joint weld 1.05 mm below the flange top surface. The positive region of Transverse distance from weld centre represents the first weld pass side, while the negative region refers the second weld pass side.
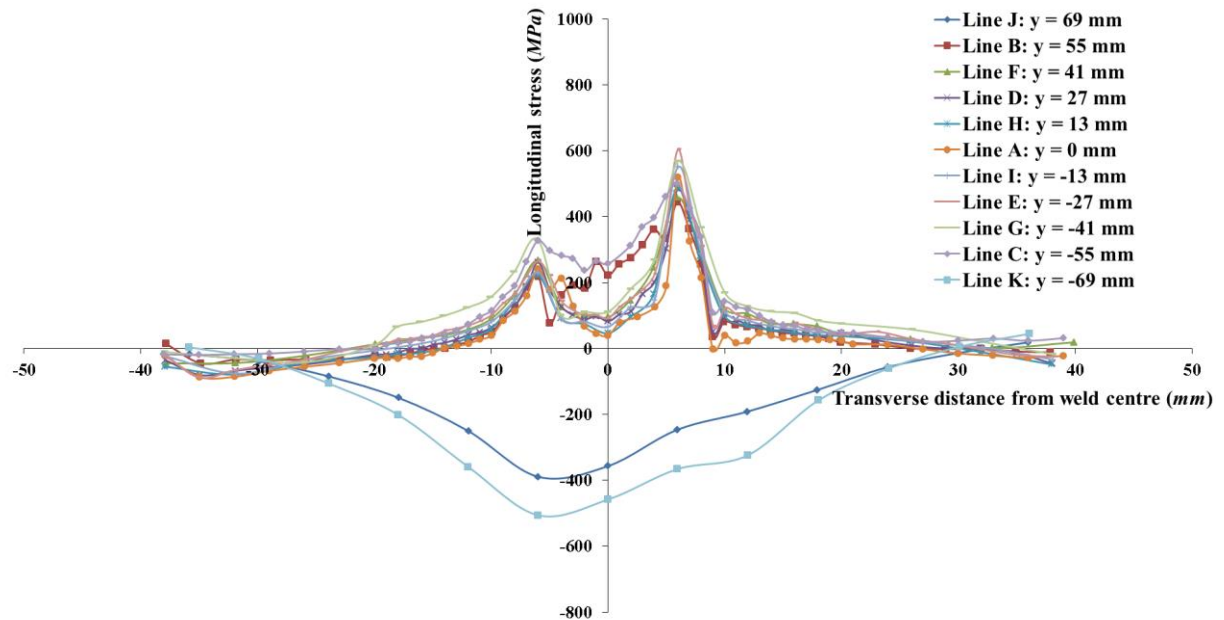

Figure 6 Transverse residual stresses along all measurement lines in Ti-6Al-4V flat T-joint weld 1.05 mm below the flange top surface. The positive region of Transverse distance from weld centre represents the first weld pass side, while the negative region refers the second weld pass side
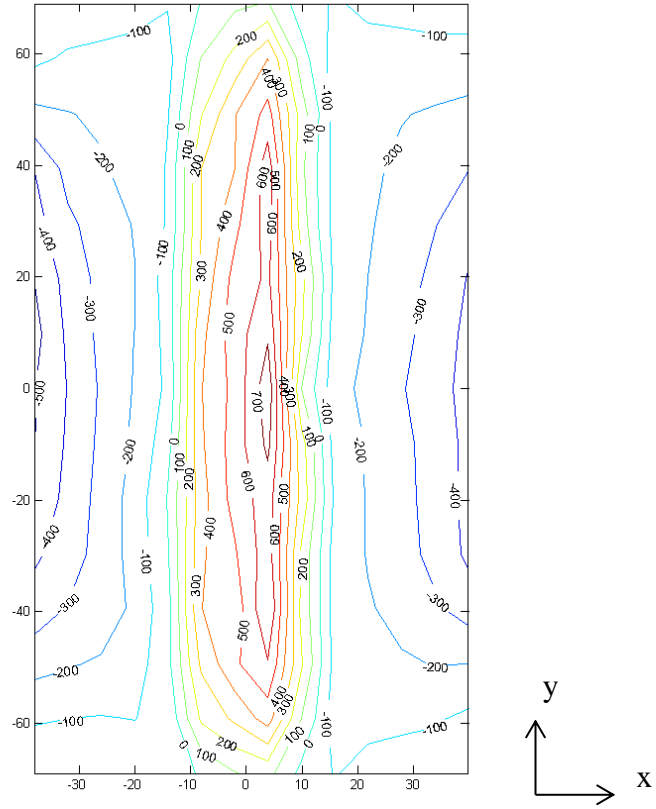
Figure 7 Contour plot of longitudinal residual stress field in Ti-6Al-4V flat T-joint weld 1.05 mm below the flange top surface. Values are in MPa.
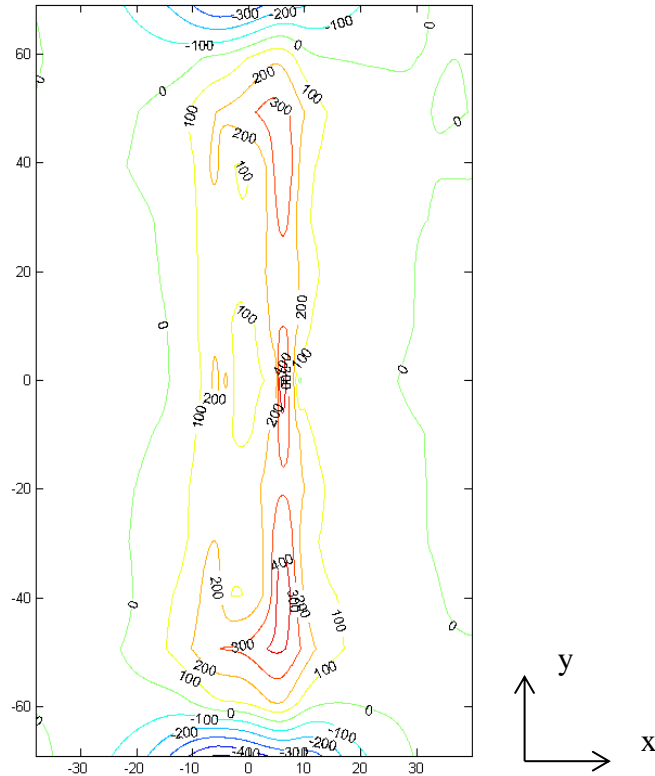
Figure 8 Contour plot of transverse residual stress field in Ti-6Al-4V flat T-joint weld at 1.05 mm below the flange top surface. Values are in MPa.

As expected, significant longitudinal residual stress variations are found in the flange, while the transverse residual stresses are very small except in the weld region. In the longitudinal direction, the tensile stress reached a maximum of 860 MPa and the peak compressive stress was at 530 MPa. As displayed in Figure 5, from the weld line to the plate's longitudinal edge, the longitudinal tensile stress climbs to a peak at a position close to the weld zone. Then it drops and turns to compression and finally achieves a maximum compressive value at the edge. However, neither clear tensile nor compressive stress variations can be found in the regions before the weld start and after the weld end. Peak values of tensile and compressive longitudinal stresses on each measurement line are plotted in Figure 9. It is clear that the magnitude of the longitudinal stress is limited by the base metal yield strength (1100 MPa [20]). Evidently the first pass area has higher tensile peaks (approximately 35% higher) but lower compressive peaks (approximately 20% lower) compared to the near second pass region. It is also evident that the maximum values in those longitudinal stress peaks occur at the middle of the plate length while the smallest peaks happen at the ends of the plate length.
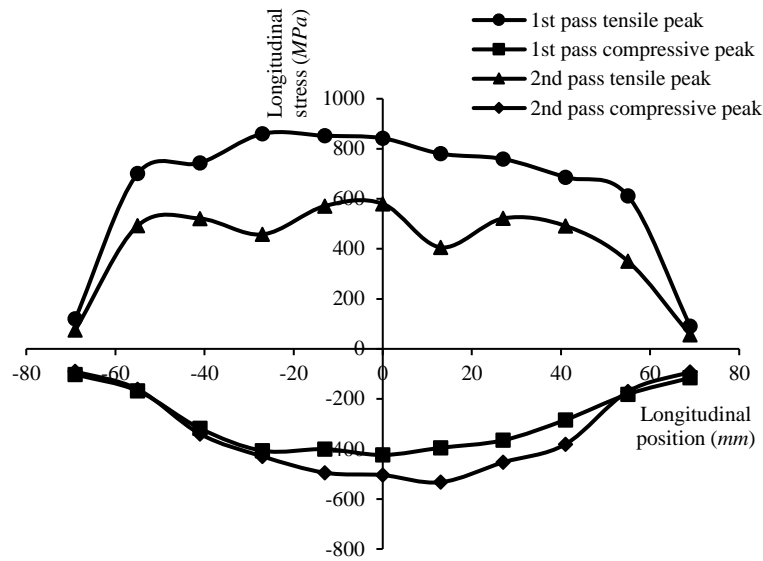
Figure 9 Peak values of tensile and compressive longitudinal residual stresses along flange length in Ti-6Al-4V flat T-joint weld at 1.05 mm below the flange top surface.

Figures 6 and 8 show that, in most of the area of the flange, the transverse residual stresses are tensile and have smaller magnitudes. Although the variations are not significant, it can still be observed at the further regions from the weld zone, the stresses are lower and there are almost no transverse stresses at the large regions near the longitudinal edges of the flange. In contrast, the areas before the weld start and after the weld end (Figure 4) produced compressive transverse stresses rather than tensile. The material in these two regions was not melted during welding and they constrained the expansion of the melted material and as a result compressive stress remained locally after the cooling.

3.2 Comparison of measured and numerical modelling predicted residual stress

The measurement results were compared to published numerical modelling results by the authors [21]. The finite element (FE) modelling was carried out using the full 3D brick elements available in the welding specific modelling software package SYSWELD, where the temperature dependent thermal mechanical properties for Ti64 used are those which were available in the software. The FE model applied identical geometries as those of the sample in the synchrotron X-ray diffraction measurement, with temperature-dependent thermo-mechanical material properties used (e.g. Young's modulus, Poisson's ratio, yield stress and plasticity stress-strain data). Figures 10 to 13 plot the longitudinal residual stress comparison between the synchrotron X-ray diffraction measured and numerical modelling predicted results.

It is evident from the figures that the predicted residual stress trends are in a good agreement with the measured ones. In the figures, it can be seen that the longitudinal residual stress pattern in both measured and predicted maps follow almost similar trends with large tensile stresses around the weld passes and compressive stresses in parent material. There are variations in the magnitude of the stresses in the negative transverse locations of the second weld pass. These variations are very likely to be the result of the lack of comprehensive set of mechanical properties available for the Ti-6Al-4V which is planned to be addressed in future

developments. The difference may also be caused by the accuracy of the residual stress measurement. ~~It should not be ignored that the presence of texture close to the weld region could make a contribution to the variation.~~ The 'comb and fish bone' shape of the d^0 sample was to relieve the stress in the material to achieve a 'strain-free' state however there is no guarantee that the stress in every tooth was fully removed. Therefore, the strain-free (d^0) sample measurement which was the reference of the stress calculation may have involved errors introduced by that. In addition, the accuracy of the measurement can be affected by operator errors, material manufacture quality, data acquisition accuracy, and other factors.
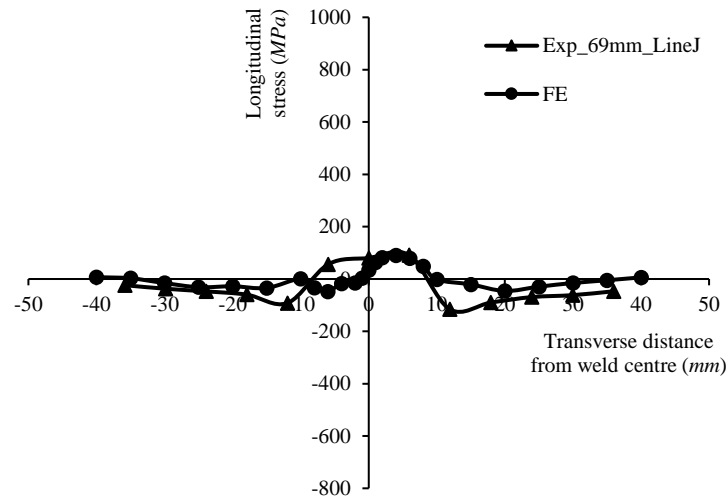

Figure 10 Ti-6Al-4V T-joint: comparison of measured and FE predicted longitudinal residual stresses along Line J. Line J is the transverse line before the weld start, 69 mm above the centre transverse line.
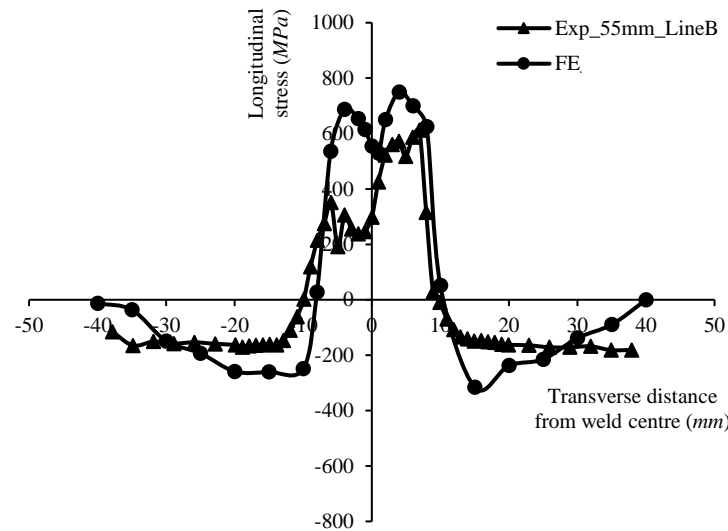

Figure 11 Ti-6Al-4V T-joint: comparison of measured and FE predicted longitudinal residual stresses along Line B. Line B is the transverse line across the weld start region, 55 mm above the centre transverse line.
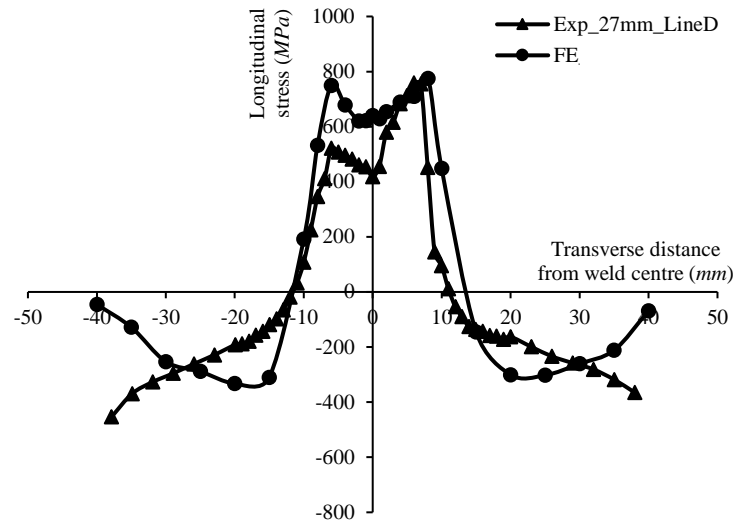
Figure 12 Ti-6Al-4V T-joint: comparison of measured and FE predicted longitudinal residual stresses along Line D. Line D is the transverse line in the middle between weld start and centre transverse Line A, 27 mm above the centre transverse line.
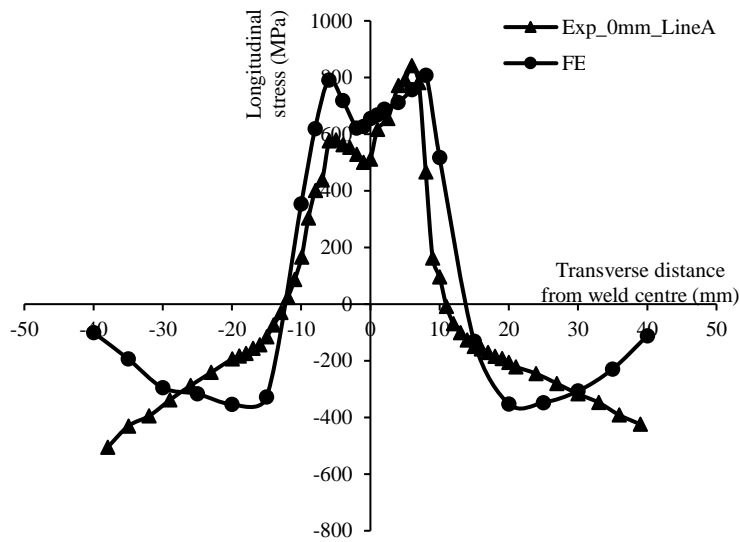

Figure 13 Ti-6Al-4V T-joint: comparison of measured and FE predicted longitudinal residual stresses along Line A. Line A is the centre transverse line through the middle of weld.

3. Concluding Remarks

The measurement of residual stresses is useful in developing welding procedures to minimise the residual stresses induced by fusion welding processes which can cause high reaction

stresses, reduced buckling strength or premature cracking for lightweight thin welded structures in aero-engines. The following conclusions can be made from this work:

> The main advantage of the high energy synchrotron X-ray strain mapping technique over the neutron strain mapping method is the speed of data collection, particularly in titanium alloys. Titanium alloys has large incoherent scattering length and small coherent scattering length for neutron, so the counting time for the same measurement is 20 minutes per point for neutron compare to 2 minutes for the synchrotron measurement.

> The disadvantage of using the energy dispersive synchrotron X-ray setup is the elongated gauge volume. For instance, incoming beam size of 0.05mm x 0.05mm with small scattering angle (2θ) of 5°, will give 1.7mm length of gauge volume in the beam direction. In previous residual stress measurement studies, thin structures were rarely investigated due to technical difficulty. The current gauge volume size makes it impossible to have more measurement positions in the through thickness direction for mapping stress variation through the thickness of the thin sheet material.

> In most of the previous studies, the measurements were carried out with a very limited number of measurement points, whereas in the present work a ~~successful~~ mapping of the complete stress fields in the welded sheets was obtained.

> The diffraction measurement results show that the longitudinal residual stresses are the most important and high tensile stresses appear at a region near the weld zone. The magnitude of the longitudinal stress is limited by the base material yield strength for the samples. In the T-joint with two partially overlapped passes, the residual stresses of the areas close to the first pass are more significant than those near the second pass. The results are in good agreement with the FE predicted results obtained in the NIMRC project work [21].

Acknowledgements

References

[1]   Feng, Z., Processes and Mechanisms of Welding Residual Stress and Distortion, 2005, London: Woodhead.

[2]   Li, M., Li, Z., Zhao, Y., Li, H., Wang, Y., and Huang, J., Influence of welding parameters on weld formation and microstructure of dual-Laser beams welded T-Joint of aluminum alloy. Advances in Materials Science and Engineering, 2011, 2011(1-6: DOI:10.1155/2011/767260).

[3]   Teng, T.L., Fung, C.P., Chang, P.H., and Yang, W.C., Analysis of residual stresses and distortions in T-joint fillet welds. International Journal of Pressure Vessels and Piping, 2001, 78(8): p. 523-538.

[4]   Deshpande, A.A., Xu, L., Sun, W., McCartney, D.G., and Hyde, T.H., Finite element based parametric study on welding induced distortion of TIG welded stainless steel 304 sheets. Journal of Strain Analysis for Engineering Design, 2011, 46(4): p. 267-279.

[5]   Deshpande, A.A., Xu, L., Sun, W., McCartney, D.G., and Hyde, T.H. Finite element modelling of heat flow and distortion in TIG welded stainless steel using SYSWELD, in AeroMat 2010 Conference, 21-24 July 2010, Bellevue, WA, United States.

[6]   Papazoglou, V.J. and Masubchi, K., Analysis and control of distortion in welded aluminum structures. Welding Journal, 1978, 57(9): p. 251-262.

[7]   Xu, L., Sun, W., McCartney, D.G., Deshpande, A.A., and Hyde, T.H. Distortion measurement of bead-on-plate and T-joint keyhole plasma arc welds of thin titanium alloy sheets, in The International Conference ESIA11 on Engineering Structural Integrity Assessment, 24-25 May 2011, Manchester, United Kingdom.

[8]   Norrish, J., Advanced Welding Processes, 1992, Bristol: IOP Pubilishing.

[9]   Noyan, I.C. and Cohen, J.B., Residual Stress: Measurement by Diffraction and Interpretation, Materials Research and Engineering, 1987, New York: Springer-Verlag.

[10] Liljedahl, C.D.M., Brouard, J., Zanellato, O., Lin, J., Tan, M.L., Ganguly, S., Irving, P.E., Fitzpatrick, M.E., Zhang, X., and Edwards, L., Weld residual stress effects on fatigue crack growth behaviour of aluminium alloy 2024-T351. International Journal of Fatigue, 2009, 31(6): p. 1081-1088.

[11] Liljedahl, C.D.M., Tan, M.L., Zanellato, O., Ganguly, S., Fitzpatrick, M.E., and Edwards, L., Evolution of residual stresses with fatigue loading and subsequent crack growth in a welded aluminium alloy middle tension specimen. Engineering Fracture Mechanics, 2008, 75(13): p. 3881-3894.

[12] Ganguly, S., Edwards, L., and Fitzpatrick, M.E., Problems in using a comb sample as a stress-free reference for the determination of welding residual stress by diffraction. Materials Science and Engineering: A, 2010, 528(3): p. 1226-1232.

[13] Ganguly, S., Figueiredo, M.A.V., and Edwards, L., Comparative neutron and synchrotron X-ray diffraction studies to determine residual stress on an as-welded AA2024 plate. Materials Science Forum, 2005, 490-491: p. 223-228.

[14] Ganguly, S., Fitzpatrick, M.E., and Edwards, L., Use of neutron and synchrotron X-ray diffraction for evaluation of residual stresses in a 2024-T351 aluminum alloy variable-polarity plasma-arc weld. Metallurgical and Materials Transactions A, 2007, 37(2): p. 411-420.

[15] Ganguly, S., Stelmukh, V., Edwards, L., and Fitzpatrick, M.E., Analysis of residual stress in metal-inert-gas-welded Al-2024 using neutron and synchrotron X-ray diffraction. Materials Science and Engineering: A, 2008, 491(1-2): p. 249-257.

[16] Ganguly, S., Pratihar, S., Fitzpatrick, M.E., and Edwards, L., Study of residual stress distribution in a stainless steel bead-on-plate simulation benchmark sample. Materials Science Forum, 2008, 571-572: p. 367-373.

[17] Korsunsky, A.M., Song, X., Hofmann, F., Abbey, B., Xie, M., Connolley, T., Reinhard, C., Atwood, R.C., Connor, L., and Drakopoulos, M., Polycrystal deformation analysis by high energy synchrotron X-ray diffraction on the I12 JEEP beamline at Diamond Light Source. Materials Letters, 2010, 64(15): p. 1724-1727.

[18] Dann, J.A., Daymond, M.R., Edwards, L., James, J. and Santisteban, J.R., A comparison between Engin and Engin-X, a new diffractomerter optimized for stress measurement. Physica B: Condensed Matter, 2004, 350 (1-3): p. 511-514.

[19] J.A. James and L. Edwards, Application of robot kinematics methods to the simulation and control of neutron beam line positioning systems. Nuclear Instruments and Methods in Physics Research A. (2007) 571, 709-718.

[20] Boivineau, M., Cagran, C., Doytier, D., Eyraud, V., Nadal, M.-H., Wilthan, B., and Pottlacher, G., Thermophysical properties of solid and liquid Ti-6Al-4V (TA6V) alloy. International Journal of Thermophysics, 2006, 27(2): p. 507-528.

[21] Sun, W., Mohammed, M.B., Xu, L., Hyde, T.H., McCartney, D.G., Leen, S.B., Process modelling and optimization of keyhole plasma arc welding of thin Ti-6Al-4V. Journal of Strain Analysis for Engineering Design. 2014, 49(6): p. 410-420.

[22] Drakopoulos, Michael, *et al*. I12: the Joint Engineering, Environment and Processing (JEEP) beamline at Diamond Light Source, Journal of Synchrotron Radiation (2015), 22, p. 828-838.